DOI: 10.1002/cctc.201000398

DFT Comparison of *N*-Nitrosodimethylamine Decomposition Pathways Over Ni and Pd

V. A. Ranea,[a, b, f] T. J. Strathmann,[c, e] J. R. Shapley,[d, e] and W. F. Schneider*[a, e]

■■please insert the academic titles of the authors■■Recent experimental studies report rapid and efficient reduction of *N*-nitrosodimethylamine (NDMA) and related aquatic micropollutants mediated by palladium (Pd) and nickel (Ni) surfaces, but differing mechanisms have been reported for the surface reactions. Here, NDMA adsorption and fragmentation on Ni and Pd surfaces has been studied using supercell slab density functional theory (DFT) calculations. NDMA adsorbs in two stable configurations on each surface. Upright binding through the NO fragment is slightly preferred energetically and provides entrance to an exothermic N–O dissociation pathway with moderately high activation barriers. Flat binding through the NNO plane is somewhat less favorable but leads to a facile and exothermic dissociation across the N–N bond. These results suggest that both mechanisms are in competition and may contribute to the observed catalytic reduction of NDMA over these metals in aqueous solution.

1. Introduction

There are growing concerns about the presence of numerous emerging classes of micropollutants in drinking water sources. The recent detection of *N*-nitrosodimethylamine (NDMA) and related *N*-nitrosamines in drinking water sources has received a great deal of recent attention because of their potent carcinogenicity[1] and other health effects including diabetes, foetal malformations, and accute tissue injury.[2] Although currently unregulated as drinking water contaminants, they are considered much more potent carcinogens than the regulated trihalomethane disinfection byproducts.[3]

Although the toxicity of NDMA has been known for many years, recent focus has resulted from studies showing its presence as a widespread aquatic contaminant due to its formation during wastewater and drinking water disinfection processes.[3] A great deal of effort is under way to understand the mechanisms and precursors controlling the formation of NDMA during these processes.[3–11] Relatively high concentrations of NDMA are formed during chlorination of wastewater that is rich in ammonia and organonitrogen precursors. This raises special concerns for municipal wastewater reuse and drinking water facilities whose source waters are impacted by upstream wastewater treatment operations.[9,12] It has also been detected in high concentrations in groundwater near rocket engine testing facilities.[3]

The concerns about NDMA have raised interest in the development of effective control technologies for water treatment and remediation. Conventional treatment techniques (biodegradation, adsorption, chemical oxidation, and air stripping) are ineffective for NDMA.[3] Currently, ultraviolet (UV) treatment is the most commonly applied NDMA treatment technology, but effective treatment requires very high levels of irradiation compared with dosages needed for disinfection.[3,13]

Recent studies have reported the rapid degradation of NDMA by metal-catalyzed reductive transformation.[14–22] Previously, rapid reduction of various *N*-nitrosamines to their corresponding amines by a variety of metals, including nickel-aluminum alloys in strong alkali (Raney Ni), has been reported.[14,15] Gui and co-workers[16,17] reported that the slow reduction of NDMA by zerovalent iron was markedly enhanced by plating 0.25 percent Ni on the surfaces of the iron grains that act as hydrogenation catalysts. More recently, Ni and Pd materials have been shown to catalyze the reduction of NDMA by exogenous hydrogen.[18,19,21,22] Catalyst activities for NDMA reduction in hydrogen-saturated solutions have been reported for Raney Ni ($78\,L\,g_{Ni}^{-1}\,h^{-1}$), nickel-boron ($30\,L\,g_{Ni}^{-1}\,h^{-1}$), granular nickel ($8\,L\,g_{Ni}^{-1}\,h^{-1}$), 1 and 5 wt% Pd on alumina support ($12\,L\,g_{Pd}^{-1}\,h^{-1}$), 1% Pd-0.3% Cu ($67\,L\,g_{Pd}^{-1}\,h^{-1}$), and 5% Pd-

[a] *V. A. Ranea, W. F. Schneider*
Department of Chemical and Biomolecular Engineering
University of Notre Dame, 182 Fitzpatrick Hall
Notre Dame, IN 46556 (USA)
Fax: (+1) 574-631-8754
E-mail: wschneider@nd.edu

[b] *V. A. Ranea*
CCT-La Plata-CONICET
INIFTA, Facultad de Ciencias Exactas, Universidad Nacional de La Plata
Calle 64 y Diagonal 113, 1900 La Plata (Argentina)

[c] *T. J. Strathmann*
Department of Civil and Enviromental Engineering
University of Illinois, Urbana, IL 61801 (USA)

[d] *J. R. Shapley*
Department of Chemistry
University of Illinois, Urbana, IL 61801 (USA)

[e] *T. J. Strathmann, J. R. Shapley, W. F. Schneider*
Center of Advanced Materials for the Purification of Water with Systems
University of Illinois, Urbana, IL 61801 (USA)

[f] *V. A. Ranea*
Current address:
INIFTA (CONICET, UNLP)
Suc. 4, C.C. 16 (1900) La Plata., Fac. de Cs. Exactas, UNLP (Argentina)

1 % In (47 $L g_{Pd}^{-1} h^{-1}$).[18,19,21,22] ■■Do you mean wt %?■■ These catalyst activities correspond to, for example, an NDMA reaction halflife of 1.5 min with 500 mg L^{-1} Raney Ni.

Although the above studies reported high activities for Ni- and Pd-containing materials, different mechanisms have been proposed for the reductive decomposition of NDMA at the metal surfaces. Lunn et al.[15] and Greene et al.[14] reported that the reduction of *N*-nitrosamines by Raney Ni in strong alkali and other metal systems proceeds by an initial N–O bond cleavage to form the corresponding hydrazine intermediate (dimethyl hydrazine for NDMA), which was subsequently reduced to ammonia and an amine (dimethylamine for NDMA) [Eq. (1)–(5)]:

$$ONN(CH_3)_2{}^{ad} \rightarrow O^{ad} + NN(CH_3)_2{}^{ad} \quad (1)$$

$$H_2{}^{ad} \rightarrow 2\,H^{ad} \quad (2)$$

$$H^{ad} + NN(CH_3)_2{}^{ad} \rightarrow N(H)N(CH_3)_2{}^{ad} \quad (3)$$

$$3\,H^{ad} + N(H)N(CH_3)_2{}^{ad} \rightarrow\rightarrow NH_3 + HN(CH_3)_2 \quad (4)$$

$$2\,H^{ad} + O^{ad} \rightarrow\rightarrow H_2O \quad (5)$$

In contrast, others report no observation of dimethylhydrazine as an intermediate in NDMA reductions at circumneutral pH in the presence of Ni- and Pd-based hydrogenation catalysts, including Raney Ni.[22] Rather, the reduction of NDMA was proposed to proceed by an initial N–N bond cleavage to form dimethylamine (DMA) and nitric oxide (NO), the latter of which is then reduced to ammonia or dinitrogen [Eq. (6)–(9)]:

$$ONN(CH_3)_2{}^{ad} \rightarrow NO^{ad} + N(CH_3)_2{}^{ad} \quad (6)$$

$$H^{ad} + N(CH_3)_2{}^{ad} \rightarrow HN(CH_3)_2 \quad (7)$$

$$4\,H^{ad} + 2\,NO^{ad} \rightarrow\rightarrow N_2 + 2\,H_2O \quad (8)$$

$$5\,H^{ad} + NO^{ad} \rightarrow\rightarrow NH_3 + H_2O \quad (9)$$

Mixtures of N_2 and NH_3 are also observed in the catalytic reduction of nitrite and nitrate over similar catalysts, and are similarly proposed to arise from intermediate generation and reduction of NO.[23–25]

In this contribution we use plane-wave, supercell density functional theory (DFT) calculations and transition-state searches to contrast the first steps in the proposed alternative mechanisms for reductive decomposition of NDMA on model Ni and Pd metal surfaces [Equations (1) and (6)]. We characterize both molecularly and dissociatively adsorbed NDMA products, as well as activation barriers for dissociation. We find that NDMA adsorbs competitively in two conformations and that each leads to different dissociation products. Dissociation across N–N and N–O bonds are both exothermic, but the former has a lower barrier on both metals. Kinetic selectivity of the N–N dissociation pathway is greater on Pd. The results are consistent with two competing dissociation pathways for NDMA on these metals.

2. Computational Details

First-principles total-energy calculations were performed using density-functional theory (DFT) as implemented in the Vienna ab initio simulation package (VASP).[26,27] The Kohn–Sham equations were solved by using the projector-augmented wave (PAW) approach for describing electronic core states[28,29] and a plane-wave basis set including plane waves up to 400 eV. Electron exchange and correlation energies were calculated within the generalized-gradient approximation (GGA) in the Perdew–Wang 91 form.[30] Atomic relaxations are considered converged when the forces on the ions are less than 0.03 eV $Å^{-1}$.

The systems were modeled by hexagonal supercells with lattice constants: $a = 7.471$ and $c = 20.334$ Å for Ni and $a = 8.390$ and $c = 22.834$ Å for Pd. The surfaces were modeled by four-layer-thick slabs separated by more than 15 Å vacuum regions to avoid interactions between the slabs. The two topmost layers were allowed to relax. A $p(3\times3)$ surface supercell was used to minimize lateral interactions. The first Brillouin-zone of the supercell was sampled with a $(6\times6\times1)$ Γ-centered mesh.

The adsorption energy is calculated as the difference between the total energy of the isolated adsorbate on ■■ok?■■ the clean, relaxed surface and the adsorbate-slab system in the optimal configuration, unless stated otherwise. We used the climbing-image nudged elastic band (cNEB) method to calculate the minimum energy pathways (MEP) and transition of states (TS) for NDMA fragmentation.[31,32] Following the construction of an initial MEP between molecular and dissociative NDMA adsorption by using linear interpolation, an initial NEB calculation was performed in order to locate the MEP. After this initial step, a cNEB calculation was used to force one image to the transition state, which was converged to 0.05 eV $Å^{-1}$.

3. Results and Discusion

3.1. Molecular NDMA adsorption

Consistent with experimental observations, calculations revealed that NDMA has a planar core, indicative of π conjugation extending across the entire molecule (Figure 1). The calculated geometric parameters compared well with experimental electron diffraction results (Table 1).[2] NDMA is both structurally and electronically similar to the parent nitrosamine, H_2NNO, and previous calculations show that the bonding can be described in terms of partial double bonds extending across N–N and N–O fragments.[33] The N–N and N–O bond lengths are consistent with this description. The calculated energies to homolytically cleave the NDMA N–N and N–O bonds are 2.60 and 4.74 eV, respectively, suggesting the former may be the more likely locus of initial decomposition. We identified both upright and flat adsorption modes on the Ni(111) and Pd(111) surfaces. As shown in Figure 1, the former is slightly energetically preferred to the latter. In this mode the adsorbate is perpendicular to the metal surface, and the N–O bond bridges two metal atoms on the surface. ■■ok?■■ Binding is stronger on the Ni surface (−0.81 eV) and the N–O and N–N bonds

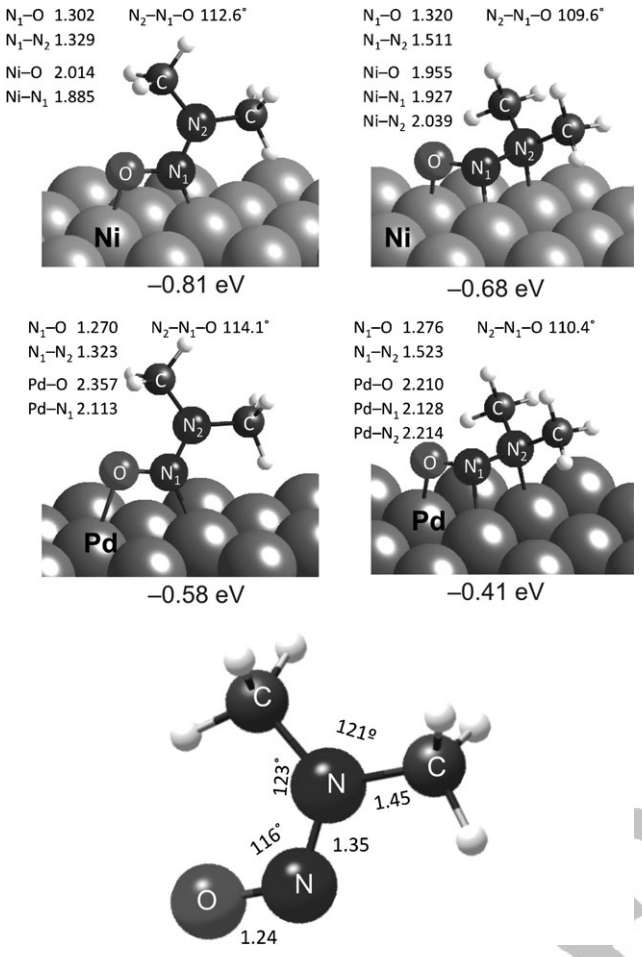

Figure 1. Computed structures of isolated and in upright and flat modes adsorbed *N*-nitrosodimethylamine (NDMA) on Ni (top) and Pd (bottom). Bond lengths in Å.

Table 1. Calculated and experimental[2] NDMA bond lengths (Å) and angles (°).

	Calculated	Experimental
O–N	1.24	1.23
N–N	1.35	1.34
N–C	1.45	1.46
C–H	1.10	
O-N-N	115.6	113.6
N-N-C	116.1	116.4
N-N-C	122.9	
C-N-C	121.0	123.2

are modified by +5 and −1%, respectively, from the gas-phase values. Binding is weaker on Pd (−0.58 eV) and bond-length variations are commensurately less. In the less-preferred flat binding mode, the O–*N*–N adsorbate plane is nearly parallel to the surface and each binds atop a surface Pd. Adsorbate distortions are greater in this mode: on Ni, the N–O and N–N bond lengths are increased by +6 and +12% from their gas-phase values and on Pd by +3 and +13%, respectively. More notably, NDMA becomes pyramidalized at the $N(CH_3)_2$ nitrogen. Adsorption energies for this flat mode are −0.68 and −0.41 eV on Ni and Pd, respectively. It is worth noting, that H_2O molecular adsorption energies at these two surfaces, calculated with the aid of a comparable model, are approximately −0.3 eV/H_2O,[34] or about half that of NDMA. We expect molecular adsorbed NDMA to compete favorably with water for surface sites.

To explore the influence of steric effects on the geometry of the NDMA adsorbate, we compared results for the less-hindered H_2NNO nitrosamine on Pd (Figure 2). Replacing methyl

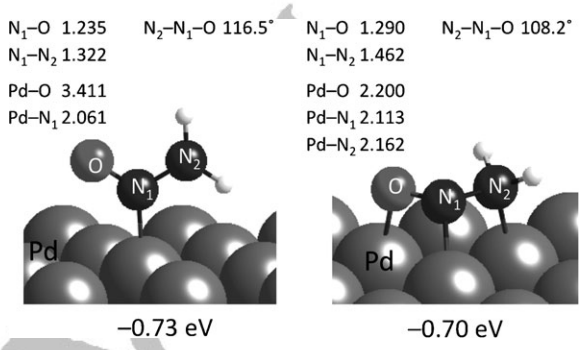

Figure 2. Computed adsorption modes of *N*-nitrosoamine on Pd.

groups with hydrogen increases the stability of both upright and flat binding modes. Without the bulkier methyl groups, the flat-bound molecule is able to approach the surface slightly more closely while decreasing the pyramidalizing distortion about the reduced N center. Adsorption is strengthened by almost 0.30 eV. Changes are even more pronounced in the upright case, where the smaller H substituent allows the adsorbate to tilt upright, binding N-down atop a single Pd, in a mode similar to atop-bound NO. Binding becomes stronger by 0.15 eV. Steric effects clearly play a role in controlling nitrosamine bonding interactions with these surfaces.

3.2. Dissociative NDMA adsorption

Figure 3 contrasts the energy surfaces for NDMA dissociation across the N–O (Reaction 1) and the N–N (Reaction 6) bonds over Pd. NDMA dissociates exothermically along either path. The N–O route produces adsorbed O and $NN(CH_3)_2$ fragments with an overall reaction energy of −1.39 eV with respect to isolated NDMA. Both products prefer to bind in three-fold hollow surface sites; $NN(CH_3)_2$ adsorbs upright with slight pyramidalization about the dimethyl N and N–N separation is essentially unchanged from its initial 1.32 Å value. The N–N path produces adsorbed NO and dimethly amine, $N(CH_3)_2$, in a route that is −1.49 eV exothermic. NO is known to bind strongly to Pd, preferably upright and linear in a three-fold site, although an atop and bent adsorption mode is also possible.[35] $N(CH_3)_2$ adopts a bridge site, straddling two surface Pd, to achieve four-fold coordination about N; binding atop a single Pd is 0.4 eV higher in energy. These results show that dissociative NDMA adsorption over Pd is quite strongly preferred over molecular adsorption, but the similar overall energetics of the two

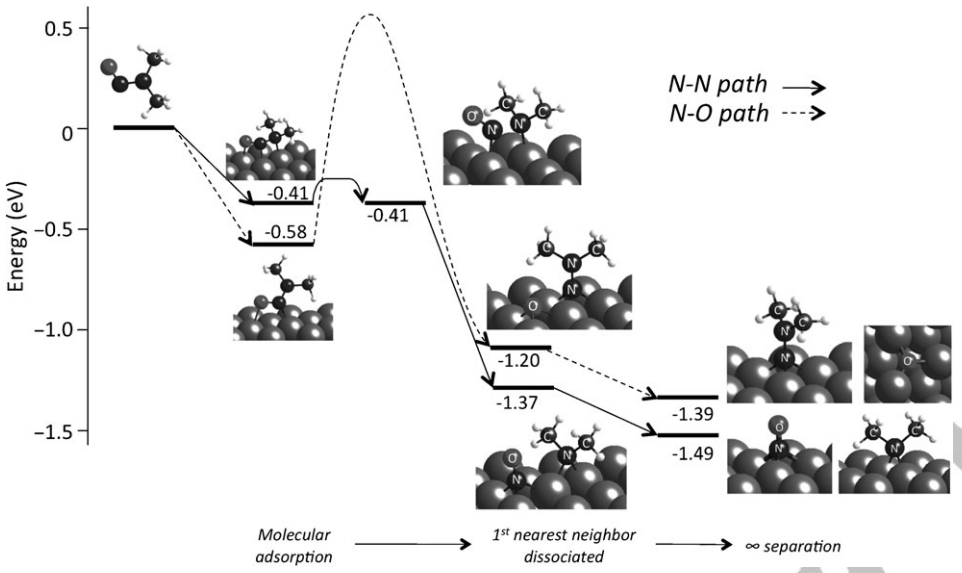

Figure 3. Calculated NDMA dissociation pathways on Pd.

dissociation pathways provides little insight into the preference for one route over the other.

To contrast the kinetics of these two reaction paths, we constructed minimum energy dissociation pathways (MEPs) and identified transition states using the nudged elastic band method (Figure 4). For the N–O route, we start from the upright-bound NDMA adsorbate and consider a path that leads to O and $NN(CH_3)_2$ products in first-nearest-neighbor three-fold sites. The MEP is initially flat, as the NDMA molecule reorients in preparation for N–O cleavage. The energy rises to the transition state in concert with a 0.5 Å stretching of the N–O bond. Past the transition state, the energy drops as the two fragments fall into their preferred three-fold coordination sites, ultimately separated by 3.2 Å. As shown in Figure 3, further diffusion of the products away from the surface lowers the energy by another 0.2 eV, a value typical of first-nearest-neighbor repulsion energies. The overall activation energy is calculated to be a substantial 1.33 eV. Diffusion barriers were not calculated here, but are expected to be substantially less than the dissociation barrier.

The N–N route begins from the flat-bound NDMA state. We identified a product state in which NO and $N(CH_3)_2$ fragments are bound atop neighboring Pd atoms, ■■ok?■■ both in a bent configuration (Figure 4). The N–N bond increases smoothly along the MEP by 0.27 Å at the transition state. The energy decreases as the fragments separate to a distance of approximately 2.0 Å, slightly closer than the underlying Pd–Pd separation. The barrier for this dissociation is a miniscule 0.06 eV. Although we verified that this is a true transition state, the barrier is small enough that factors not included in the model, such as interference from the aqueous environment, may have a significant effect on the absolute rate. With reference to Figure 3, moving the products from this atop-atop configuration to the preferred first-nearest-neighbor three-fold sites lowers the energy an additional 1 eV. As noted above, NO and $N(CH_3)_2$ prefer three-fold sites but can also adopt atop binding sites; this geometrical flexibility is likely to aid relaxation of the initially formed dissociation intermediate. ■■ok?■■

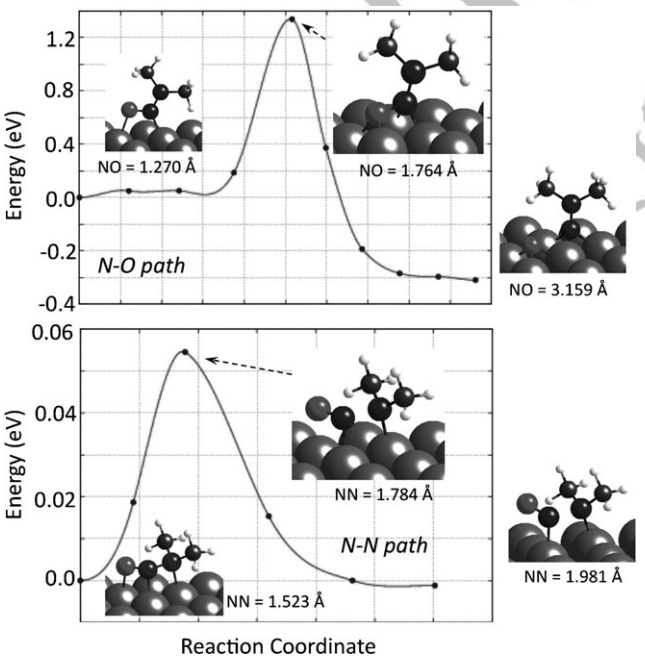

Figure 4. NEB-calculated NDMA dissociation barriers on Pd.

Comparing these two results, we see that the N–N dissociation pathway has a substantially smaller activation energy than the N–O pathway. A cautious comparison of the Arrhenius factors indicates that at room temperature the N–N route would be 21 orders of magnitude faster than the N–O route. Given the simplicity of the models of the interface and the computational and theoretical uncertainties in the computed barriers, the DFT results strongly suggest a decomposition mechanism dominated by the dimethylamine (DMA)+NO route over Pd. ■■ok?■■

Shown in Figure 5 is the computed energy landscape for the decomposition of NDMA over Ni. The first thing to note is the large difference in energy scales between Figures 3 and 5. Ni binds NDMA itself and all dissociation intermediates more strongly than Pd, and dissociation across either the N–O or the N–N bond is quite exothermic. Although the N–O path is slightly less favorable energetically over Pd than over Ni, it is 0.9 eV more exothermic than the N–N dissociation on Ni and more than twice as exothermic as the N–N dissociation on Pd. ■■ok?■■ These trends reflect the high oxophilicity of the Ni surface; most of the difference between Pd and Ni can be

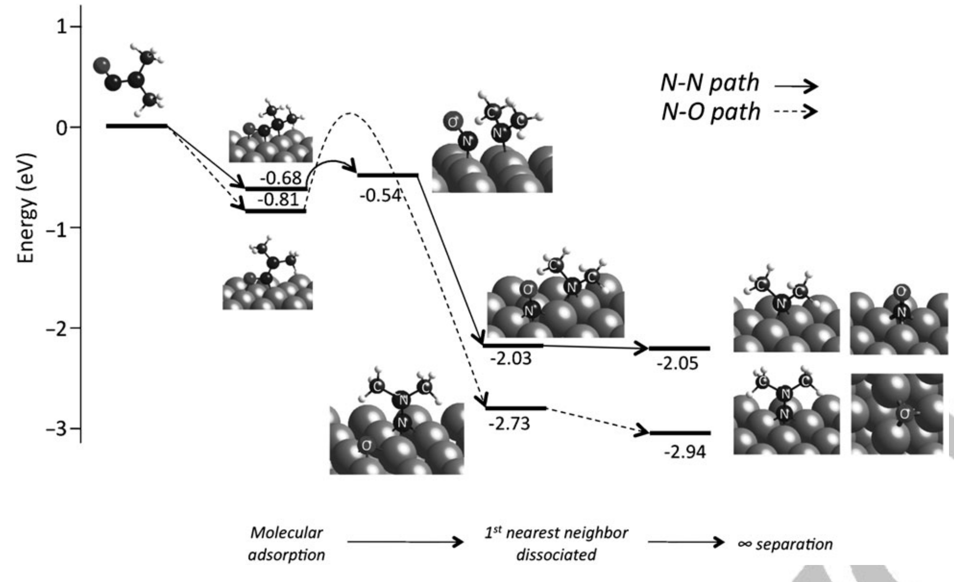

Figure 5. Calculated NDMA dissociation pathways on Ni.

attributed to the 1 eV greater binding energy of O to the latter. Despite the difference in energetics, product structures are similar to those identified on Pd. The N–N route also leads to product states similar to those found on Pd, but here the energy change from metal to metal is a more moderate 0.5 eV, consistent with the more moderate difference in NO adsorption energies between Pd and Ni. Thus, for Ni, energy considerations favor dissociation across the N–O bond over the N–N bond dissociation.

As with Pd, we used the NEB method to search for transition states along the N–O and N–N dissociation paths (Figure 6). Results are again qualitatively similar to Pd. The N–O route proceeds from upright-bound NDMA and terminates with $NN(CH_3)_2$ and O products in first-nearest-neighbor three-fold sites. The greater overall exothermicity of the N–O cleavage pulls the transition state down in energy, so that the activation barrier decreases to 0.56 eV. Diffusion of products away from neighboring sites lowers the energy by another 0.2 eV. The N–N route shifts in the opposite direction. Again, the MEP proceeds from flat-bound NDMA and terminates with NO and $(CH_3)_2$ fragments in first-nearest-neighbor atop sites, with a N–N separation of 1.63 Å at the transition state and a final N–N separation of 1.93 Å. The smaller Ni lattice constant causes these numbers to decrease in comparison to the Pd case, and repulsive neighbor interactions thus push both transition and final states up in energy. The dissociation barrier over Ni is 0.23 eV, still moderate but four-times larger than over Pd. These atop fragments relax into nearest-neighbor three-fold sites, lowering the energy by 1.5 eV. Further diffusion to greater separations has minimal effect on the energy.

Over Ni, the N–N cleavage has a lower barrier than N–O, but the difference between the two is much less than on Pd, in large parts because of the quite exothermic adsorption of O on Ni. The overall activation energies of both pathways are relatively moderate, however, and these results are consistent with both pathways contributing to NDMA decomposition over Ni.

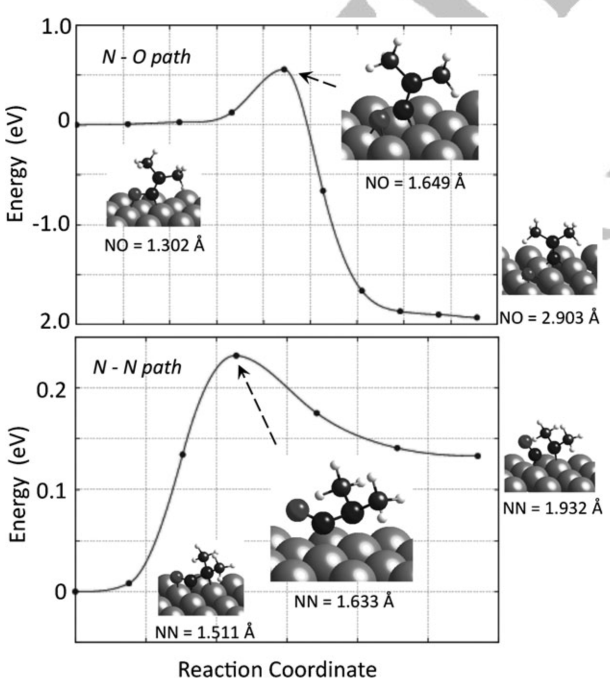

Figure 6. NEB-calculated NDMA dissociation barriers on Ni.

4. Conclusions

Supercell DFT calculations show that NDMA molecularly adsorbs at Pd and Ni surfaces with moderate adsorption energies and in two competing adsorption configurations. Dissociative adsorption by means of Equation (1) or Equation (6) is exothermic on both surfaces. Over Pd, dissociation across the N–O bond produces adsorbed dimethylhydrazine and O. N–O bond dissociation has a considerably higher activation barrier than the dissociation across the N–N bond, which produces dimethylamine and NO. Kinetics thus appear to favor the N–N dissociation route over Pd catalysts. The situation is more complex over Ni: the strong affinity of Ni for O decreases the activation energy along the N–O cleavage route, whereas the smaller Ni lattice constant pushes up the N–N dissociation barrier. The latter remains kinetically preferred, but by a sufficiently small amount that both pathways are likely to compete. The preferred route over Ni is thus likely dependent on the catalytic details: particle morphology, coverage of adsorbates, and composition of the reaction environment. The results show

that such features must be taken into careful consideration when accessing competing reaction mechanisms.

The results indicate that NDMA decomposition is facile over either metal without the direct participation of hydrogen as a reductant. Although the calculations are performed in the absence of any solvating water, it is likely that, given the very strong decomposition tendencies, this conclusion is robust to the inclusion of H_2O. Water and especially hydrogen clearly play important roles in the subsequent reduction of the decomposition products, and the overall kinetics of reduction to N_2 or NH_3 are likely to be determined by reaction steps beyond the NDMA dissociation. Current work in our group focuses on elucidating these subsequent reduction steps.

Acknowledgements

This work was supported by WaterCAMPWS, a Science and Technology Center program of the National Science Foundation under Agreement CTS-0120978.

Keywords: catalytic reduction · density functional calculations · nickel · palladium · water pollutants

[1] *Toxicological Profile for* N-*nitrosodimethylamine*. Agency for Toxic Substances and Disease Registry, **1989**, U.S. Public Health Service in collaboration with the U.S. EPA.
[2] *The chemistry of amino, nitroso and nitro compounds and their derivatives, Part 2* (Ed.: S. Patai), Wiley, **1982**.
[3] W. A. Mitch, A. C. Gerecke, D. L. Sedlak, *Water Res.* **2003**, *37*, 3733 – 3741.
[4] W. A. Mitch, D. L. Sedlak, *Environ. Sci. Technol.* **2004**, *38*, 1445 – 1454.
[5] W. A. Mitch, D. L. Sedlak, *Environ. Sci. Technol.* **2002**, *36*, 588 – 595.
[6] J. Choi, R. L. Valentine, *Water Res.* **2002**, *36*, 817 – 824.
[7] J. Choi, S. E. Duirk, R. L. Valentine, *J. Environ. Monit.* **2002**, *4*, 249 – 252.
[8] E. Pehlivanoglu-Mantas, D. L. Sedlak, *Water Res.* **2006**, *40*, 1287 – 1293.
[9] E. Pehlivanoglu-Mantas, A. L. Hawley, R. A. Deeb, D. L. Sedlak, *Water Res.* **2006**, *40*, 341 – 347.
[10] I. M. Schreiber, W. A. Mitch, *Environ. Sci. Technol.* **2005**, *39*, 3811 – 3818.
[11] W.-H. Chen, T. M. Young, *Environ. Sci. Technol.* **2008**, *42*, 1072 – 1077.
[12] S. W. Krasner, P. Westerhoff, B. Chen, B. E. Rittmann, S.-N. Nam, G. Amy, *Environ. Sci. Technol.* **2009**, *43*, 2911 – 2918.
[13] S. Liang, J. F. G. J. H. Min, M. K. Davis, D. S. Remer, *J. Am. Water Works Assoc.* **2003**, *95*, 121 – 131.
[14] B. Greene, M. B. McClure, H. T. Johnson, *Chem. Health Saf.* **2004**, *11*, 6 – 13.
[15] G. Lunn, E. B. Sansone, L. K. Keefer, *Carcinogenesis* **1983**, *4*, 315 – 319.
[16] L. Gui, R. W. Gillham, M. S. Odziemkowski, *Environ. Sci. Technol.* **2000**, *34*, 3489 – 3494.
[17] M. S. Odziemkowski, L. Gui, R. W. Gillham, *Environ. Sci. Technol.* **2000**, *34*, 3495 – 3500.
[18] A. J. Frierdich, J. R. Shapley, T. J. Strathmann, *Environ. Sci. Technol.* **2008**, *42*, 262 – 269.
[19] M. G. Davie, M. Reinhard, J. R. Shapley, *Environ. Sci. Technol.* **2006**, *40*, 7329 – 7335.
[20] C. H. Schaefer, C. Topoleski, M. E. Fuller, *Water Environ. Res.* **2007**, *79*, 57 – 62.
[21] M. G. Davie, K. Shih, F. A. Pacheco, J. O. Leckie, M. Reinhard, *Environ. Sci. Technol.* **2008**, *42*, 3040 – 3046.
[22] A. J. Friedrich, C. E. Joseph, T. J. Strathmann, *Appl. Catal. B* **2009**, *90*, 175 – 183.
[23] U. Prüsse, M. Hähnlein, J. Daum, K.-D. Vorlop, *Catal. Today* **2000**, *55*, 79 – 90.
[24] S. D. Ebbesen, B. L. Mojet, L. Lefferts, *J. Catal.* **2008**, *256*, 15 – 23.
[25] S. D. Ebbesen, B. L. Mojet, L. Lefferts, *Langmuir* **2008**, *24*, 869 – 879.
[26] G. Kresse, J. Hafner, *Phys. Rev. B* **1994**, *49*, 14251 – 14269.
[27] G. Kresse, J. Furthmüller, *Phys. Rev. B* **1996**, *54*, 11169 – 11186.
[28] P. Blöchl, *Phys. Rev. B* **1994**, *50*, 17953 – 17979.
[29] G. Kresse, J. Joubert, *Phys. Rev. B* **1999**, *59*, 1758 – 1775.
[30] J. P. Perdew, J. A. Chevary, S. H. Vosko, K. A. Jackson, M. Pederson, D. Singh, C. Fiolhais, *Phys. Rev. B* **1992**, *46*, 6671 – 6687.
[31] G. Henkelman, B. P. Uberuaga, H. Jónsson, *J. Chem. Phys.* **2000**, *113*, 9901 – 9904.
[32] H. Jónsson, G. Mills, K. Jacobsen in *Classical and Quantum Dynamics in Condensed Phase Simulations*, (Eds: B. J. Berne, G. Ciccotti, D. F. Coker) World Scientific, **1998**, 385 – 404■■ok?■■.
[33] D. Sun, W. F. Schneider, J. B. Adams, D. Sengupta, *J. Phys. Chem. A* **2004**, *108*, 9365 – 9374.
[34] A. A. Phatak, W. N. Delgass, F. H. Ribeiro, W. F. Schneider, *J. Phys. Chem. C* **2009**, *113*, 7269 – 7276.
[35] M. Gajdos, J. Hafner, A. Eichler, *J. Phys. Condens. Matter* **2006**, *18*, 13 – 40.■■ok?■■

Received: November 10, 2010
Published online on ■■ ■■, 0000

Figure it out: DFT calculations are used to contrast the contributions of N–N and N–O bond cleavage to the catalytic reduction of the environmental pollutant *N*-nitrosodimethylamine (NDMA).

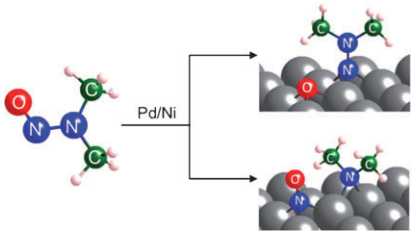

*V. A. Ranea, T. J. Strathmann, J. R. Shapley, W. F. Schneider**

■■ – ■■

DFT Comparison of *N*-Nitrosodimethylamine Decomposition Pathways Over Ni and Pd

